Carbon Research

ORIGINAL ARTICLE

Open Access

Check for updates

Variations in redox properties of biochar and humic acid induced by interactive molecular exchange

Shasha Li[1,3], Pinjing He[3], Hua Zhang[1,2], Liming Shao[2,3] and Fan Lü[1,2]*

Abstract

Biochar and humic substances are prevalent redox pools in the environment, which is critical to electron transfer in geochemical cycles and pollution control processes. The dissolution of biochar and the sorption of humic substances on biochar have the potential to redistribute redox substances, consequently altering the redox properties of solid and liquid phases. However, studies have often focused on either sorption or dissolution separately, overlooking the mutual effects and not involving redox properties. Herein, molecular interactions between biochar and humic acid (HA) and variations in their redox properties were elucidated using UPLC Orbitrap MS and mediated electrochemical measurement. The dissolution of biochar was far greater than the sorption of HA constituents, and HA enhanced the dissolution of biochar through molecular exchange. But preferential sorption of oxygenated aromatics to pine char (pi500) mainly by hydrogen bonding and higher saturated molecules to starch char (st700) mainly by hydrophobic interactions caused the oxygenated functional groups on biochar to increase (1 ~ 1.5 times). Thus the Electron exchange capacities (EEC) of pi500 and st700 turned to 1 ~ 3 times, and the EEC of HA decreased ca. 50%. Absorption (partition) caused more sorption of HA constituents to pi500 than to st700, while larger surface area resulted in higher EEC of st700 with sorbed HA. The enrichment of redox constituents on biochar is promising for its long-term use in waste reclamation and pollution control. The findings can aid in the understanding of variations in redox properties under interactions between pyrolytic and natural organic matter.

Highlights

- The dissolution of biochar was far more than the sorption of HA constituents.
- Dissolution of biochar was enhanced by humic acid through molecular exchange.
- Sorbed redox constituents increased biochar EEC to 1~3 times.
- Oxygenated aromatics were sorbed to pine biochar mainly by hydrogen bonding.
- Higher saturated molecules were sorbed to starch biochar mainly by hydrophobic interactions.

Keywords Pyrolytic carbon materials, Natural organic matters, Electron exchange capacities, Sorption, Dissolved black carbon

---

*Correspondence:
Fan Lü
lvfan.rhodea@tongji.edu.cn
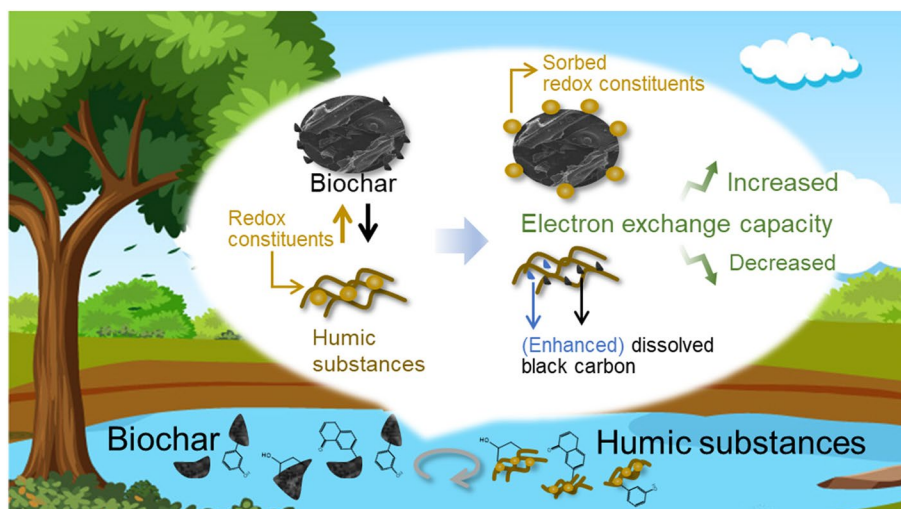Full list of author information is available at the end of the article

 Springer

Li *et al. Carbon Research*   (2024) 3:26

Page 2 of 13

Graphical Abstract

1 Introduction

Biochar is a carbonaceous material derived from the pyrolysis of biomass which has been increasingly utilized for resource reclamation, pollution control, and climate change mitigation (Lehmann et al. 2021; Yang et al. 2020). The role of biochar in facilitating electron transfer is well recognized to contribute a lot to the redox transformation of contaminants (Wang et al. 2022; Yu et al. 2015) and waste valorization (Cruz Viggi et al. 2017; Shao et al. 2019) during these applications. Meanwhile, the functions of biochar are closely associated with the redox properties which are derived from redox-active moieties (Cruz Viggi et al. 2017). Humic substances are ubiquitous organic matters in the environment, also processing redox properties like biochar and being able to act as electron shuttles for redox reactions like biochar (Aeschbacher et al. 2012, 2010; Guo et al. 2018; Lee et al. 2019). Therefore, redox properties play critical roles in functions of biochar and humic substances in mediating electron transfer and affecting the geobiochemical redox cycles (He et al. 2022; Sun et al. 2017).

Once biochar is applied to the natural environment or artificial microbial reactors, sorption of organics or dissolution of biochar fractions will occur. The sorption-dissolution behavior will bring changes to the physicochemical properties of biochar, thus affecting subsequent redox properties and functions of biochar in the niches. For instance, it was reported that co-composted biochar was coated by complex organic matter and hence the plant growth was more promoted by co-composted biochar than by pristine biochar (Hagemann et al. 2017). But another research discovered the co-composted biochar loaded with nitrogenated matters showed less enhancement than un-composted biochar during agronomic application (Kaudal and Weatherley 2018). Majority of the above organic matter are humic substances, which are highly transformed natural organic matter widely persisting in biochar applied environments, such as soil, marshes and swamps, and municipal sewage sludge (Lipczynska-Kochany 2018), compost (Qi et al. 2022) and digestate (Guilayn et al. 2020). In addition, the dissolved fractions of biochar will enter into liquids. It has been estimated that the forest output $5 \sim 7 \times 10^4$ tons of dissolved biochar to rivers annually (Dittmar et al. 2012). And the dissolved biochar fractions are mostly highly functionalized with phenol/aromatic ether C−O, alkene C=C/amide C=O, polysaccharides C−O, and alcohol/ether/carbohydrate C−O groups (Song et al. 2023), which have been proved to be redox-active (Li et al. 2020). Thus, the dissolution might cause redox-active molecules to run off from biochar particle.

Redox properties could be quantified by electron exchange capacities (EEC) consisting of electron-donating capacities (EDC) and electron-accepting capacities (EAC). Preferential sorption of natural organic matter on aluminum oxide could cause the EEC of dissolved and adsorbed fractions to change (Subdiaga et al. 2020, 2019). Biochar also shows polarity with the presence of noncarbon atoms, and thus, when biochar is added to humic substance-rich environment, sorption of organic constituents onto biochar probably affects the EEC of humic substances. And the dissolved fractions of biochar

Li *et al. Carbon Research*   (2024) 3:26

Page 3 of 13

will become part of the humic substances and induce potential changes into the EEC of them. Thereby, as the abundant organic substances in nature, the interactions between biochar and humic substances can be essential to the redox pool.

Although the sorption of humic substances (Kasozi et al. 2010; Shi et al. 2020) onto biochar has been investigated, there is a lack of elucidation in sorption-dissolution coexistence behavior and fate of redox-active substances. Additionally, the subsequent effects on the redox properties of biochar and humic substances were not considered. Moreover, previous research on the dissolution of black carbon into acid, alkaline solution or organic liquid (Qu et al. 2016; Song et al. 2021) cannot reflect the additional effects of humic substances on dissolution processes. Thus, this work was intended to investigate the molecular evolution during bidirectional interactions of sorption and dissolution using ultra-performance liquid chromatography coupled with Orbitrap mass spectrometry (UPLC Orbitrap MS), the respective structural and constituent changes of biochar and humic acid, and the subsequent changes in redox properties of solid and liquid phases. The findings can provide understanding of the long-term changes in the redox properties of biochar applied in organic environment.

2 Materials and methods

2.1 Material preparation

Biochars were prepared according to previous research (Klüpfel et al. 2014; Li et al. 2020). The pine-wood biochars were derived from pine wood pyrolyzed at 500 °C and possessed relatively higher EEC (Klüpfel et al. 2014). The starch-derived biochars pyrolyzed at 700 °C under nitrogen flow of 1 L/min showed an outstanding surface area and EEC in comparison to chars derived from other biomass components (Li et al. 2020). As EEC was decided by both surface area and redox-active moieties, the two types of biochar were selected because both exhibit excellent EEC but differ in terms of surface area, and the two chars have opposite spatial distribution of redox-active moieties within the biochar particles, as discovered in our previous work (Li et al. 2023). The chars pyrolyzed from pinewood and starch were labeled as pi500 and st700, respectively. Both chars were ground by mortar and pestle and then passed through a 200-mesh sieve (< 75 μm). The atomic proportion (obtained by X-ray photoelectron spectroscopy), BET specific area and EEC of pristine biochar are shown in Table S1.

ABTs (2,2'-azino-bis[3-ethylbenzothiazoline-6-sulfonic acid] diammonium salt, ≥ 98.0%, CAS: 30,931–67-0) and diquat dibromide monohydrate (analytical standard, CAS: 6385–62-2) were purchased from Sigma Aldrich, China. Humic acid (HA) was used to represent humic

substance with concern that HA represents a large portion of natural organic matter in soils, sediments and waters (Shaker and albishri 2014). HA purchased from Sigma Aldrich was dissolved in Millipore deionized water by adjusting the solution to alkaline, and then 1 M HCl was titrated until pH reached 7.0 to prepare a HA stock solution of 200 mg/L. The stock solution was stored in the dark under 4 °C and was filtered by membranes (0.45 μm, Whatman, Germany) before subsequent use.

2.2 Interaction experiments

HA stock solution was purged with nitrogen for 45 min and then diluted into six concentrations (5, 20, 40, 60, 80, and 100 mg/L). 0.5 g of biochar was mixed with 50 mL diluted HA solution. The control treatments had 0.5 g of biochar mixed with 50 mL ultrapure water (Millipore, USA) for comparison. The experiments and control treatments were all conducted in triplicate. Samples were periodically collected and the pH was manually adjusted to 7.0 by 0.1 M KOH or HCl during sample collection until apparent equilibrium. Apparent equilibrium of interactions was indicated by constant pH and dissolved organic carbon (DOC) of solution samples filtered by membranes (0.45 μm, Whatman, Germany). All the operations were conducted in an anaerobic glovebox (AW400SG/TG, Electrotek, UK; oxygen < 1 ppm). The sealed vessels were vibrated by a rotator in a dark incubator at 20 °C (YC-80, Hangzhou Miu Instruments Co.Ltd).

2.3 Mediated electrochemical analysis

The EDC and EAC of HA stock solution, filtrates and suspensions (containing biochar and HA solution) in interaction equilibrium were determined by mediated electrochemical oxidation and reduction, respectively. The EEC of biochar in interaction equilibrium was calculated by the electron difference between the suspensions and corresponding filtrates. All the measurements were carried out at least in triplicate and the outliers were removed according to Grubbs' test with a significance level of 0.01. The detailed procedures were provided in Text S1, Supplementary Information.

2.4 Characterization of biochar and biochar-HA complex

The biochar-HA complex after interactions were centrifuged, and then dried for 24 h at 40 °C for subsequent X-ray photoelectron spectroscopy analysis, in order to recognize the changes in functional groups of biochar induced by interactions with HA solution. The spectra recorded by X-ray photoelectron spectroscopy (XPS, AXIS Ultra DLD, Kratos Analytical Ltd, Japan) were deconvoluted into several peaks by XPS Peak Fit software for C 1s and O 1s. C 1 s spectrum was fitted into sp^2 (284.6 eV), sp^3 (285.2 eV), C–O (286.8 eV), C=O

Li *et al. Carbon Research*   (2024) 3:26

Page 4 of 13

(288.9 eV), and π-π* (291.0 eV) peaks (Varga et al. 2017). O 1 s spectrum was fitted into quinone (531.2 eV), C=O (532.5 eV), C–OH (533.7 eV) (Wang et al. 2018), and – COOH (534.3 – 535.4 eV) peaks (Chen et al. 2018). The BET surface area of pristine biochar was determined by a nitrogen adsorption method using a surface area and porosity analyzer (ASAP 2460, Micromeritics Instrument Corp., United States).

2.5 Characterization of HA

The DOC of filtered suspension during sorption and dissolution processes was detected using a TOC analyzer (TOC-VCPH, Shimadzu, Japan). Excitation-emission matrix (EEM) fluorescence spectra of the filtrates were obtained using a fluorescence spectrometer (Cary Eclipse, Agilent, USA). The filtrates were diluted until the $SUVA_{254}$ values were less than 0.3 L/(mg·m) to avoid inner filter effects (Subdiaga et al. 2019). $SUVA_{254}$ is the specific UV–vis absorbance at 254 nm calculated by the formula ($SUVA_{254} = Abs_{254} \times 100 / DOC$), where Abs_{254} is UV–vis absorbance at 254 nm measured using 1 cm quartz cuvettes and a UV–vis spectrophotometer (UV-1800, Shimadzu, Japan). EEM spectra were scanned under a range of emission (Em 280 ~ 520 nm) and excitation (Ex 200 ~ 400 nm) wavelengths with scan steps of 2 nm and 10 nm, respectively. EEM data were preprocessed in the order of excluding noisy or contaminated wavelengths, removing scatter peaks and parts, removing outlier samples, normalizing the dataset, and then decomposed by parallel factor analysis (PARAFAC) using Matlab toolbox (drEEM) according to the detailed tutorial in a previous publication (Murphy et al. 2013). The exported maximum intensity of the components (Fmax) was correlated with the relative amount of the corresponding component. Split half analysis and residual analysis were used for validating a PARAFAC model (Stedmon and Bro 2008).

2.6 UPLC Orbitrap MS analysis

The molecular characteristics of HA stock solution and filtrates in equilibrium were analyzed using ultra-performance liquid chromatography coupled with Orbitrap mass spectrometry (UPLC Orbitrap MS, Q-Exactive Plus, Thermo Fisher Scientific, USA). A C18 column was equipped for separation; electrospray ionization (ESI) was used for the ionization of molecules in positive (ESI+) and negative (ESI−) mode; and the analysis conditions referred to our previous publication (Qiu et al. 2020; Shao et al. 2021). All the samples were determined in triplicate. The pretreatment procedures of samples are depicted as follows. The concentration and desalination of samples were performed by solid-phase extraction (SPE) using PPL (a styrene–divinylbenzene copolymer, 1 g, 6 mL, Agilent, USA) according to the difference in polarity between inorganic salts and organic matters. The pH of samples was pre-adjusted to around 2 using 1 M HCl to protonate acidic functional groups, decrease polarity, and improve stationary phase binding (Bahureksa et al. 2021). The SPE cartridges were rinsed with 1 cartridge volume of methanol (HPLC grade, ≥ 99.9%, Sigma-Aldrich), and then rinsed with 2 cartridge volumes of 0.01 M HCl for the re- equilibrium. Samples were passed through the cartridges at a flow rate of 5 mL/min, and the cartridges were subsequently rinsed with at least 2 cartridge volumes of 0.01 M HCl to remove the salt. The cartridges were dried with air and adsorbed organics were eluted with 1 cartridge volume (6–40 mL) methanol at a flowrate of < 2 mL/min (Dittmar et al. 2008; Qiu et al. 2020). The eluates were stored in the dark at −20 °C before UPLC Orbitrap MS analysis. Eluate aliquots were dried by a vacuum freezing dryer, and then dissolved in ultrapure water to determine the carbon recovery of samples during SPE using a TOC analyzer (TOC-VCPH, Shimadzu, Japan).

2.7 Molecular information analysis

Compound Discoverer 3.2 (Thermo Fisher Scientific, Inc., USA) was used for the analysis of mass spectra to calculate molecular formulas (mass error < 5 ppm). The obtained formulas were validated based on the chemical constraints (Text S2). The molecules which did not meet the constraints and existed in the control samples were excluded. Only when a formula exists in more than two replicates was it considered to be included in the sample. Moreover, the molecules were classified into 7 categories according to H/C and O/C ratios (Shao et al. 2021; Smith et al. 2013; Yuan et al. 2017), and the detailed classifications were provided in Text S3. Molecular indexes including molecular weight (MW), H/C, O/C, modified aromaticity index (AImod), double bond equivalence (DBE), and nominal oxidation state of carbon (NOSC), were calculated to reflect molecular characteristics according to Text S4 (Shao et al. 2021). AImod, DBE, and NOSC can indicate the aromaticity, degree of unsaturation, and redox state, respectively (Zhang et al. 2021). Peak-area weighted averages of molecular indexes for a sample can indicate the overall molecular characteristics of the sample (Text S4).

3 Results and discussion

3.1 DOC and EEM changes during interaction processes

As shown in Fig. S1a-b, the DOC of filtered suspension for all treatments (including the control groups) increased and then got steady over time, indicating that the dissolution amount of the dissolved fractions of biochar surpassed the sorption amount of

Li *et al. Carbon Research*　　(2024) 3:26

Page 5 of 13

HA constituents. Additionally, after deducting the DOC values in the control group dissolved from biochar, the DOC of experimental groups with relatively higher HA concentration still increased (Fig. S1c-d), indicating that the presence of HA promoted the dissolution of biochar. Meanwhile, the higher increase of DOC (Fig. S1) illustrated that the dissolution of pi500 exceeded that of st700, which can be ascribed to the combination of feedstock and pyrolysis temperature. Because pine wood char released relatively more dissolved organic matter than chars from corncob, corn straw and bamboo (Han et al. 2021), and more aliphatic carbons and unstable organics existed in biochar pyrolyzed at a lower temperature (Smith et al. 2016; Taherymoosavi et al. 2017).

However, for DOC results, the adsorption of HA to biochar was shielded by the dissolution of biochar. Therefore, fluorescent technique was used to distinguish the changes of HA substances. EEM spectra were decomposed into one component (Fig. S2), and the Fmax can reflect the relative concentration of HA. Thus, Fmax values (Fig. 1) were used to fit the sorption isotherms instead of the conventional method that is based on DOC concentrations. The Freundlich model (Kasozi et al. 2010) based on the fitting of the absorbed HA was selected for best simulation (coefficients of determination, $R^2 = 0.986$). The modified Freundlich affinity

coefficient (k) for pi500 is 1.3 times that for st700, showing HA had more affinity to pi500 than st700.

3.2 Percentage of sorbed and dissolved molecules

Molecular information was obtained by UPLC Orbitrap MS analysis. Sorption percentage of molecules was calculated according to methods in Text S5. The sorption percentages of sorbed molecules in 5 mg/L of HA were all 100%, and sorption percentages of only about 20 in more than 1000 sorbed molecules in 100 mg/L of HA did not reach 100%. Therefore, the molecules that were not totally sorbed were counted as not sorbed hereafter. The identified molecules were classified into 6 categories based on sorption and dissolution characteristics (Table S3): 1) HA constituents that were totally sorbed (sorbed), 2) HA constituents that remained in the filtrates at equilibrium (remained), 3) HA constituents that were transformed or dissolved black carbon of which the dissolution was inhibited by HA (changed); 4) molecules shared by HA and dissolved black carbon (shared); 5) molecules only existing in dissolved black carbon (biochar); 6) molecules that were generated from the reactions between biochar and HA or enhanced dissolution (generated). The proportion of molecules for each category in HA and dissolved black carbon were shown in Fig. 2. 75% and 69.4% of molecules in HA were sorbed by pi500 in ESI- and ESI+ modes, respectively, while 23.7%
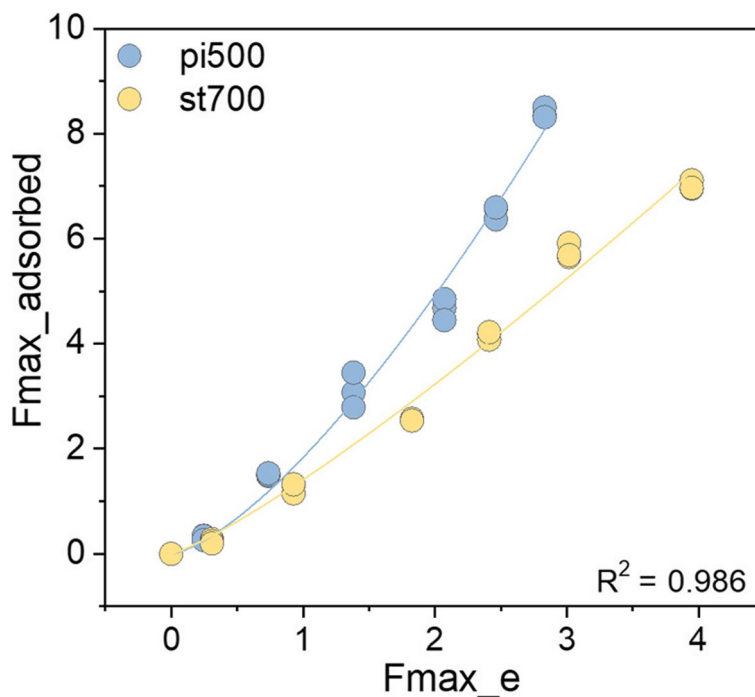
Fig. 1 HA sorption isotherms on biochar. "pi" and "st" represent the chars derived from pine wood and starch, respectively. The number suffixes represent pyrolysis temperatures. Solid lines represent Freundlich model fitting

Li *et al. Carbon Research*   (2024) 3:26

Page 6 of 13
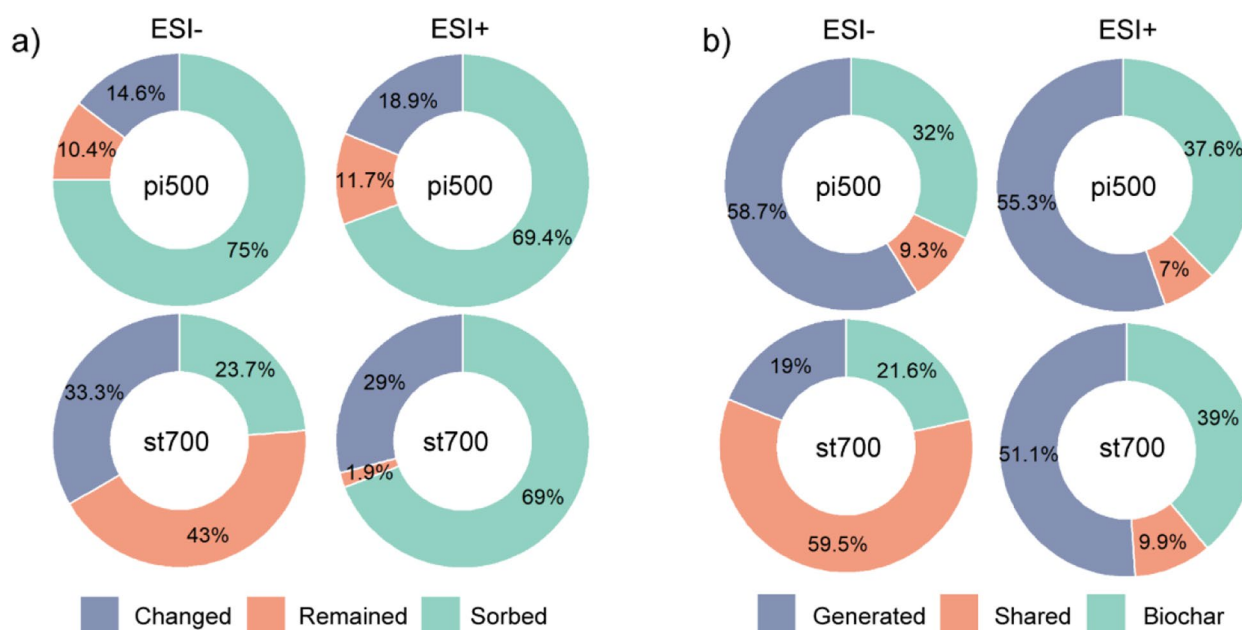
Fig. 2 Proportion of molecules for each category in HA and dissolved black carbon. **a** Proportion of molecules in HA which were sorbed, changed by biochar and molecules which remained in the filtrates at equilibrium; **b** proportion of molecules which were both shared in dissolved biochar and HA, unique in biochar, and newly generated from the interactive reactions or enhanced dissolution. "pi" and "st" represent the chars derived from starch and pine wood, respectively. The number suffixes represent pyrolysis temperatures

and 69% of molecules in HA were sorbed by st700 in ESI- and ESI + modes, respectively. This revealed that the sorption of HA by pi500 were higher than that by st700. Additionally, molecules generated from reactions or enhanced dissolution of pi500 (58.7% and 55.3% in ESI- and ESI + modes, respectively) were more abundant than those of st700 (19% and 51.1% in ESI- and ESI + modes, respectively).

3.3 Changes of molecules in HA solution after interactions with biochar

The identified molecules were classified into different categories according to elemental composition and van Krevelen diagram (Fig. S3). The majority of the molecules were identified in ESI + mode, indicating that most molecules tend to subtract a H atom or add an electron (Kujawinski and Behn 2006). This is consistent with CHO, lipids, and lignin categories dominating in all the samples. The counts of assigned formulas in the categories are shown in Fig. S4. The assigned formulas in the filtrates at the equilibrium of interactions between HA and pi500 were more than HA stock solution, in accord with the stronger dissolution than sorption of pi500. According to the count of assigned formulas, the dissolved molecules from pi500 mainly belonged to CHO, CHON (Fig. S4), while the relative intensity of CHOS dominated (Fig. S5). As for the molecular categories, the dissolved

molecules from pi500 mainly belonged to lignin/CRAM-like, aliphatic/proteins, and lipids (Fig. S4-5). The peak-area weighted averages of molecular indexes (Table S2) showed that O_{wa}, O/C_{wa}, DBE_{wa}, and $(AImod)_{wa}$ of HA were higher while H_{wa} and H/C_{wa} were lower than those of filtrates after interactions with pi500. Besides, the H/C of sorbed molecules was significantly lower ($p < 0.05$) than dissolved ones, while the O/C, NOSC, and AImod were significantly higher ($p < 0.05$). This indicated that unsaturated aromatic and oxygenated compounds in HA were sorbed after interactions and the dissolved molecules contained more hydrogen contents than HA and sorbed molecules, also consistent with the dissolution of lipids and aliphatics. The counts of assigned formulas in filtrates after interactions between HA and st700 were fewer than those in HA and the control group, indicating the preference for sorption and changes in dissolved molecules induced by HA. The little change in DOC after deduction of dissolution (Fig. S1) showed that the sorbed DOC was comparable to the dissolved DOC facilitated by HA. The counts of assigned formulas and relative intensity revealed that the sorbed molecules to st700 belonged to lipids and the dissolved molecules from st700 belonged to CHO, lignin/CRAM-likes, and aliphatic/proteins. In addition, the DBE of sorbed molecules was less than the dissolved ones, indicating that molecules of higher saturation were sorbed.

Li *et al. Carbon Research*   (2024) 3:26

Page 7 of 13

3.4 Changes in EEC and surface functional groups of biochar after interactions

The EEC were calculated by integrating current peaks illustrated by Fig. S6-9. Both the EDC and EAC of biochar in equilibrium became higher than those of biochar in the control group, and increased with the weight ratios of HA to biochar and then got steady (Fig. 3). For the groups with 100 mg/L HA, the EDC and EAC of pi500 became 1.63-fold (13.37 ± 0.81 μmol e⁻/g vs. 8.20 ± 1.01 μmol e⁻/g) and 1.15-fold (72.34 ± 2.70 μmol e⁻/g vs. 63.15 ± 4.30 μmol e⁻/g) compared with biochar in the control group, respectively. The EDC and EAC of st700 became 2.67-fold (63.01 ± 3.84 μmol e⁻/g vs. 23.60 ± 8.97 μmol e⁻/g) and 1.45-fold (504.3 ± 48.9 μmol e⁻/g vs. 347.6 ± 67.0 μmol e⁻/g) compared with biochar in the control group, respectively. It is noted that the EDC of biochar in the control group in equilibrium became much lower than pristine biochar (23.6 ± 9.0 μmol e⁻/g vs. 201.2 ± 21.0 μmol e⁻/g for st700; 8.2 ± 0.8 μmol e⁻/g vs. 21.7 ± 2.5 for pi500) and the EDC of filtrates at equilibrium was below detection, which can result from the permeation of oxygen into the vessels.

Biochar interacted with 5 mg/L and 100 mg/L HA were selected to characterize changes of surface functional groups as determined by XPS (Fig. S10). The proportion of C 1s, O 1s, and N 1s categories were calculated based on the relative amount of peak area and illustrated in Fig. 4. Compared with biochar in the control groups, the C 1s categories of biochar in equilibrium were similar,

indicating the little change in the carbon structure of biochar. The oxygenated groups (including C=O, C–O, and –COOH) were elevated after interaction with HA. For the groups with 100 mg/L of HA, the proportions of C=O, C–O, and –COOH in st700 became 1.30, 1.53, and 1.18 times as the control group, respectively, while those in pi500 became 1.42, 1.23, 1.27 times as the control group, respectively. The proportion of quinones in pi500 was elevated to 1.42 times. Furthermore, the oxygenated groups of pi500 and st700 in 5 mg/L of HA were similar to those in control groups, suggesting that the increase of functional groups was related to concentrations of HA, and sorption of substances containing such groups was probably the reason (Kasozi et al. 2010). On the contrary, pyrrolic-N of st700 and pi500 decrease during the interactions with HA. For the groups with 5 mg/L of HA, the proportions of pyrrolic-N in st700 and pi500 decreased to 71% and 35% of the control groups, respectively. For the groups with 100 mg/L of HA, the proportions of pyrrolic-N in st700 and pi500 decreased to 42% and 52% of the control groups, respectively.

Based on the analysis of molecular changes in the solution, the increase of oxygenated groups on pi500 resulted from the sorption of oxygenated and aromatic molecules as well as the dissolution of more saturated aliphatic molecules. Given that EDC and EAC are positively correlated with C–O and quinone/C=O (Li et al. 2020), respectively, the EDC and EAC were subsequently elevated. Although the oxygenated functional groups on st700
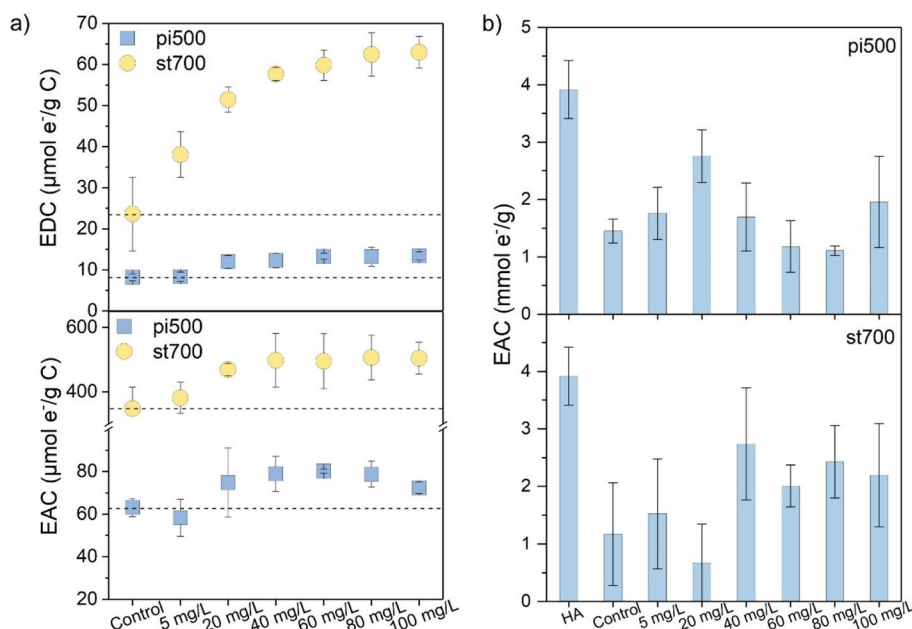
Fig. 3 EEC of **a**) biochar and **b**) HA stock solution and filtrates at equilibrium. "pi" and "st" represent the chars derived from pine wood and starch, respectively. The number suffixes represent pyrolysis temperatures. The dashed lines represent values of control groups
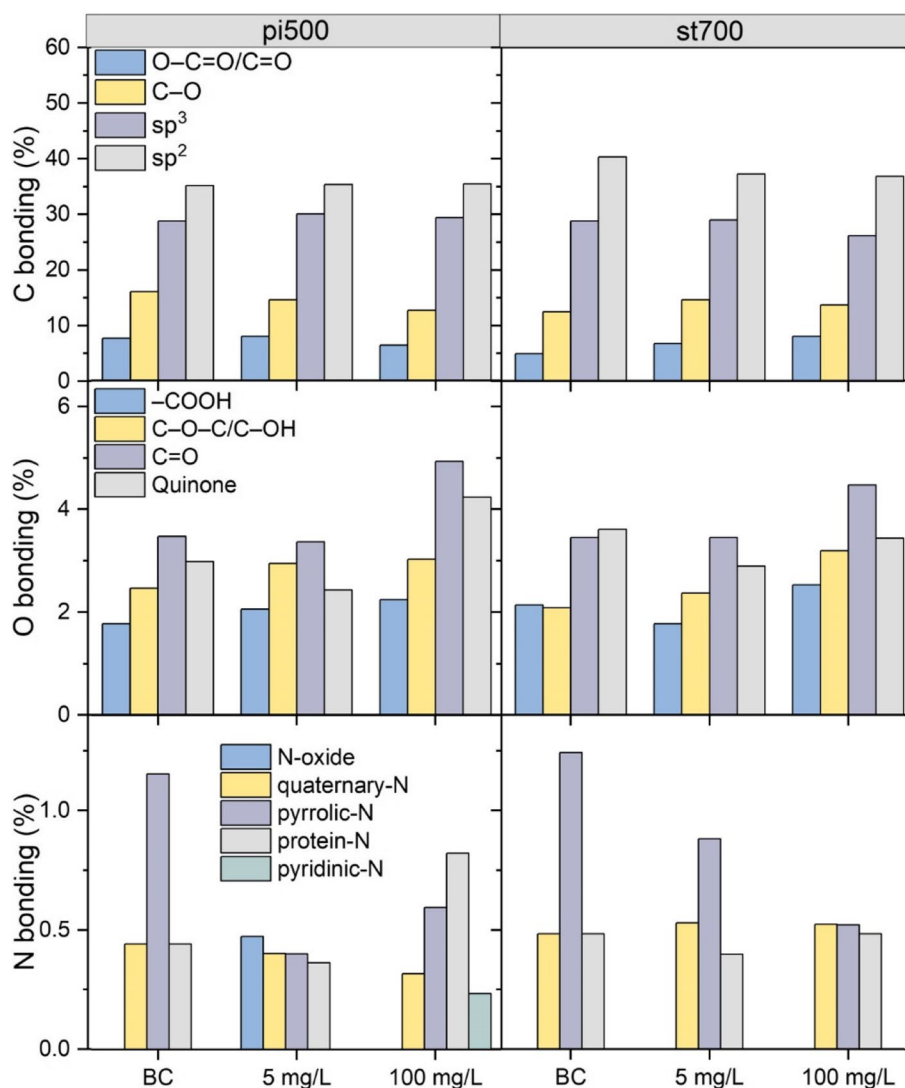
Fig. 4 Proportion of C 1s, O 1s and N 1s bonding of biochar. "pi" and "st" represent the chars derived from pine wood and starch, respectively. The number suffixes represent pyrolysis temperatures. "BC" represents biochar in the control groups

were elevated after interaction with HA, the O contents did not express a significant difference ($p > 0.05$) between sorbed and dissolved molecules, which can result from the low mass of sorption. Comparing between st700 and pi500, the increasing folds of both EDC and EAC of st700 exceeded pi500. Combined with the weaker sorption of st700 than pi500, this phenomenon can be attributed to the larger surface area of st700 expanding the exposure of sorbed molecules (Li et al. 2020).

### 3.5 Effects of interactions on the constituents and redox properties of HA

The dissolved substances from biochar possessed EAC (1.17 mmol e⁻/g C for dissolved st700; 1.45 mmol e⁻/g

C for pi500), while the EAC of filtrates in equilibrium decreased compared with HA stock solution (3.91 mmol e⁻/g C). Combined with the increasing EAC of biochar after interactions, this illustrates the net sorption of electron-accepting constituents from HA onto biochar. The changes in HA induced by biochar can be analyzed by combining the difference in dissolved molecules and HA constituents (Fig. 6) with the difference in sorbed and dissolved molecules (Fig. 5). Comparing the molecules shared by pi500 and HA with unique molecules dissolved from pi500 (Fig. 6), we found that the dissolution of pi500 would induce molecules with lower C contents, H/C, molecular weight, but higher NOSC and aromaticity. Because the sorbed molecules possess more oxygen

Li *et al. Carbon Research*   (2024) 3:26

Page 9 of 13
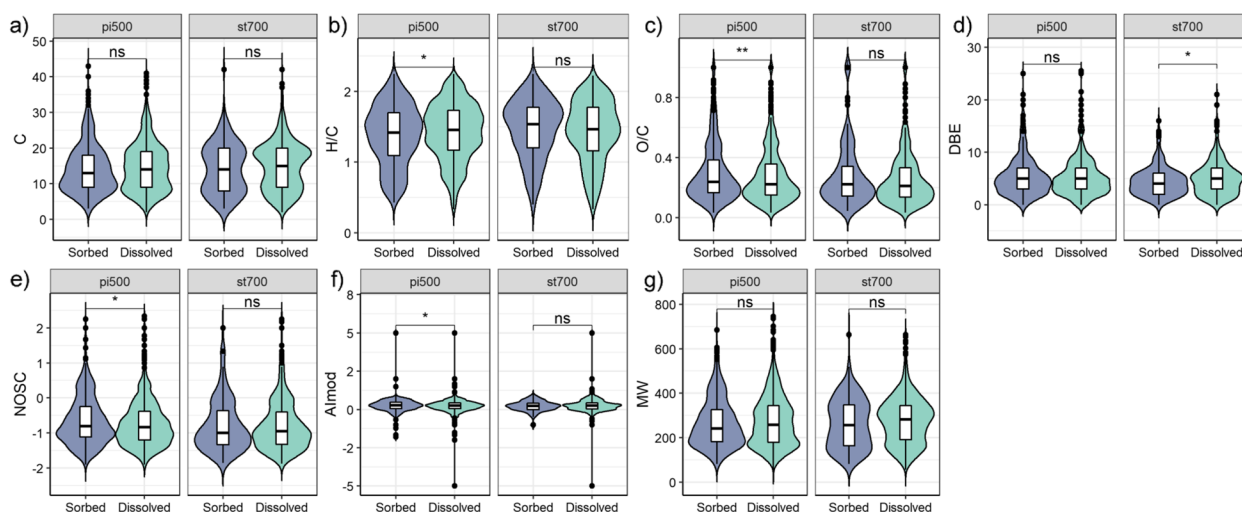
Fig. 5 Molecular indexes of sorbed and dissolved molecules. *, **, *** represent the presence of significant differences, where *, **, and *** correspond to $p < 0.05$, $p < 0.01$, $p < 0.001$, respectively. ns represents no significant differences (Wilcoxon test). "pi" and "st" represent the chars derived from pine wood and starch, respectively. The number suffixes represent pyrolysis temperatures
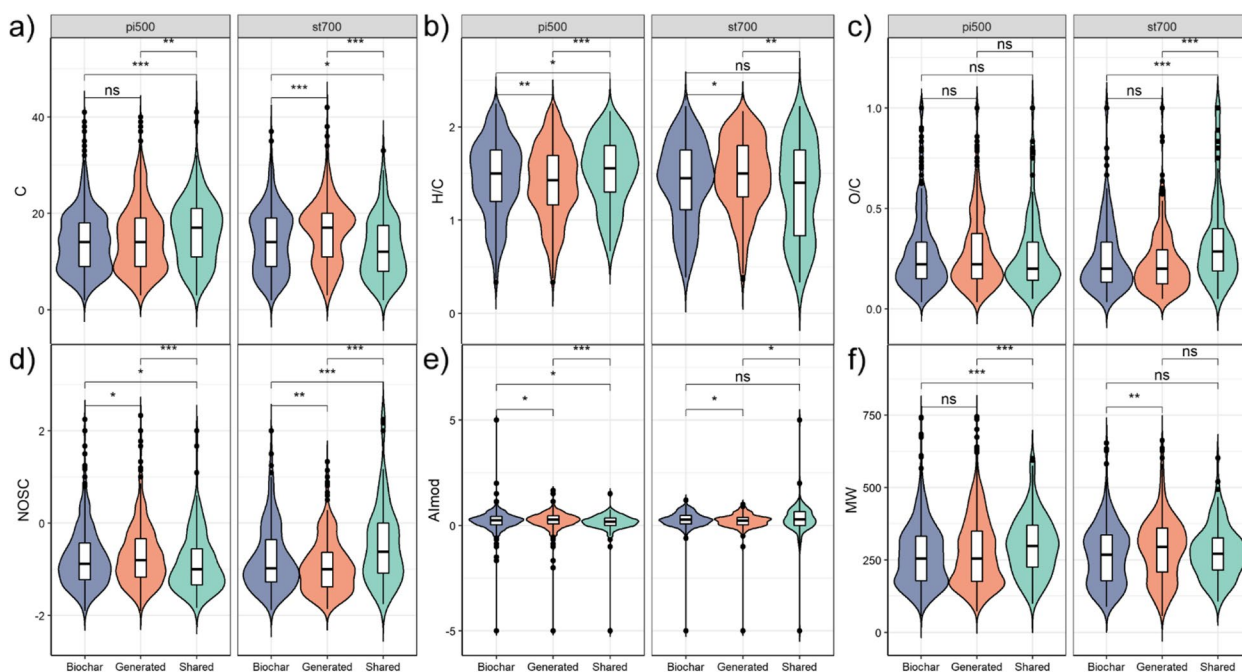
Fig. 6 Molecular indexes of dissolved molecules. *, **, *** represent the presence of significant differences, where *, **, and *** correspond to $p < 0.05$, $p < 0.01$, $p < 0.001$, respectively. ns represents no significant differences (Wilcoxon test). "pi" and "st" represent the chars derived from pine wood and starch, respectively. The number suffixes represent pyrolysis temperatures

contents and aromaticity than dissolved ones (Fig. 5), the interactions will bring down the oxygen contents and aromaticity of HA. This can be supported by the lower Owa, O/Cwa, DBEwa, and (AImod)wa of filtrates than those of HA (Table S2). Combining the increase of C=O on pi500 with the decrease of EAC during interactions,

it can be deduced that the sorption of oxygenated molecules by pi500 caused C=O in HA to decrease. The EDC of filtrates was below the detection limit, but the decrease of oxygenated molecules in HA, and the increase of C–O and EDC of biochar implied that the EDC of HA would drop. The molecules induced by st700 contained more C

Li *et al. Carbon Research*   (2024) 3:26

Page 10 of 13

contents, lower O/C and lower NOSC (Fig. 6), combined with the increasing oxygenated functional groups of st700, suggesting that the oxygenated molecules enriched on the biochar from HA, which can be the reason why the EEC of HA decreased (Li et al. 2020).

4 Discussion

4.1 The presence of HA-enhanced dissolution of biochar

The dissolved molecules from biochar enhanced by HA can be analyzed by comparing the molecules generated from reactions or enhanced dissolution and the dissolved black carbon in the control groups (Fig. 6). Reactions would not cause DOC to increase, but the DOC after deduction of dissolved DOC in control groups still increased, revealing that HA indeed enhanced the dissolution of some molecules from biochar. Compared with dissolved black carbon in the control groups, dissolved molecules from pi500 enhanced by HA contained lower H/C but higher NOSC and AImod; while dissolved molecules from st700 enhanced by HA contained more carbon, H/C, and higher molecular weight but lower NOSC and lower AImod. This indicates that HA promoted the dissolution of more oxygenated aromatics from pi500 and more saturated molecules from st700. It's noted that the dissolved molecules enhanced by HA from pi500 and st700 turned to be totally different from the normally

dissolved ones that were hydrogenous molecules from pi500 and higher carbonaceous molecules from st700, but similar to the sorbed molecules to the corresponding biochar, respectively. This suggests that the enhancement of dissolution by HA resulted from molecular exchange, which means that HA constituents displaced the molecules previously present on biochar. The molecular indexes of molecules, the dissolution of which was changed by HA, fell in the range between those of sorbed and remaining molecules (Fig. 7), which means the sorption bindings between them and biochar were at the critical point. Thus, it is reasonable that the bindings can be affected by HA.

4.2 Mechanisms for the preferential sorption of HA constituents on biochar

Adsorption and absorption (partition) often simultaneously existed during the sorption of organics to biochar, because biochar contains carbonized fractions as adsorbent phase and noncarbonized fractions as partition phase (Chen et al. 2008; Chun et al. 2004). From the above, HA constituents displaced the molecules previously present on biochar, indicating the presence of adsorption, as the displacer would not impede the solute uptake by a partition process (Chiou et al. 2015). The presence of preferential sorption of HA constituents can
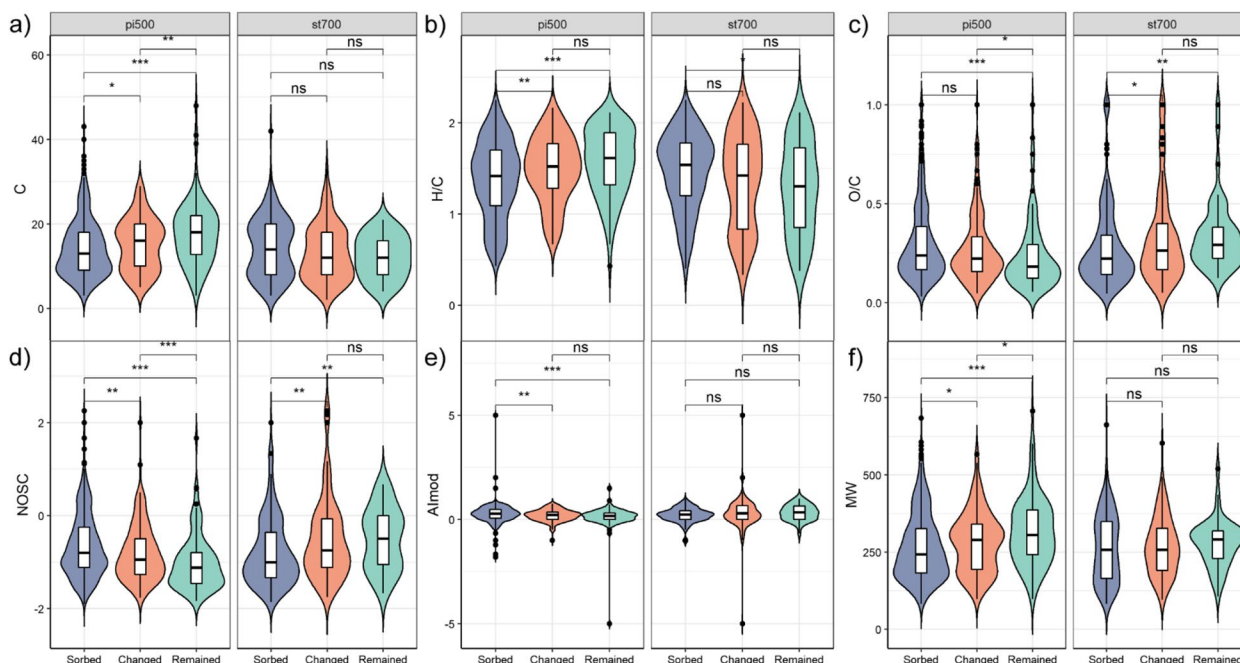
Fig. 7 Molecular indexes of molecules in HA which were sorbed, changed by biochar and molecules which remained in HA. *, **, *** represent the presence of significant differences, where *, **, and *** correspond to $p < 0.05$, $p < 0.01$, $p < 0.001$, respectively. ns represents no significant differences (Wilcoxon test). "pi" and "st" represent the chars derived from pine wood and starch, respectively. The number suffixes represent pyrolysis temperatures

Li *et al. Carbon Research*   (2024) 3:26

Page 11 of 13

be recognized by comparing the sorbed molecules and molecules remaining in the filtrates after interactions (Fig. 7). Molecules containing lower C, H/C, molecular weight but higher O/C, NOSC, and aromaticity were preferentially sorbed by pi500; while molecules containing higher H/C but lower O/C and NOSC were preferentially sorbed by st700. This is consistent with the above findings that pi500 sorbed oxygenated aromatics (polar substances), while st700 sorbed more saturated molecules containing less oxygen (hydrophobic lipids). Known from the analysis of XPS spectra (Fig. 3), the relative contents of sp^2 hybridized carbon, quinone, C=O, and carboxyl group on st700 are higher than those on pi500, while pi500 contains more sp^3 hybridized carbon and C—O. It is indicated that hydrogen bonding is the main adsorption mechanism for pi500 and hydrophobic interactions dominated in HA adsorbed to st700 (Shi et al. 2020). In this work, biochar sorption isotherms become highly linear at higher concentrations for both pi500 and st700, indicating the presence of absorption (Kasozi et al. 2010). Besides, the sorption of HA to pi500 was higher than that to st700, whereas the specific surface area of st700 (294.8 m^2/g) was 3.67 times that of pi500 (80.4 m^2/g) (Table S1). This can be ascribed to more absorption for HA to pi500, because of the presence of more noncarbonized fractions as suggested by the relative content of sp^3 hybridized carbon (Chen et al. 2008), and the dissolution of pi500 that caused sorption vacancies can be the reason for more sorption of HA to pi500 (Kasozi et al. 2010).

4.3 Implications

The selected biochars (pi500 and st700) were chosen due to the excellent EEC and the opposite spatial distribution of redox-active moieties caused by different pyrolysis mechanisms (unreacted-core-shrinking approximation for pine wood, decomposition and condensation for starch) (Li et al. 2023). In our previous work (Li et al. 2023), redox-active moieties increase from outside to inside of pi500 particles, while those of st700 decrease. For biochar with these different characteristics, the interactions didn't cause redox-active moieties of both biochar to transport into HA solution, but preferentially sorbed different molecules and had both the EECs promoted, and HA enhanced both to dissolve molecules whose characteristics were similar to the referentially sorbed ones, suggesting the universality of these phenomena.

The present study demonstrated that although more organic matters entered into the liquid phase during the interactions between biochar and HA, the redox constituents in HA were selectively sorbed onto biochar, inducing variations in redox properties of both the solid and liquid phases. Given that both HA and biochar can act as redox mediators in the environment and they often co-exist in an environmental system, e.g., soil, sediment, compost, anaerobic reactors and wastewater treatment tanks, the redox substances in these systems will be redistributed and preferentially sorbed to biochar. Thus, the redox constituents will become enriched in solid phases, which is encouraging for the long-term use of biochar in waste reclamation and pollution control. Meanwhile, the findings also provide a new perspective that the redox properties of biochar can be elevated using HA that is ubiquitous and readily accessible in the environment. Furthermore, environmental factors, such as pH, play an important part in molecular interactions and redox states, but the present study only took the neutral condition for example, hence further investigation in the effects of these factors is still required.

5 Conclusions

The molecular redistribution between HA and biochar and the resulting changes in redox properties were clarified. The increase in DOC resulting from the dissolution of biochar molecules far exceeded the decrease in DOC resulting from sorption. And HA turned out to enhance the dissolution of biochar molecules in the water phase through molecular exchange. Specifically, HA promoted the dissolution of more oxygenated aromatics from pi500 and more saturated molecules from st700. Additionally, oxygenated aromatics were preferentially sorbed to pi500 mainly through hydrogen bonding, while more saturated molecules containing less oxygen were preferentially sorbed to st700 by hydrophobic interactions, resulting from the polar surface of pi500 (containing C=O, C–O, and sp^3) and more carbonized surface of st700 (more sp^2 and quinone). Absorption (partition) caused more sorption of HA constituents to pi500 than to st700, while larger surface area resulted in higher EEC of st700 with sorbed HA. Overall, the selective sorption of HA constituents caused the increase of oxygenated functional groups (C=O, C–O, –COOH, quinone) on both pi500 and st700, leading to increase in the EEC of biochar (1 ~ 3 times) and decrease in the EEC of HA. This study observed simultaneous dissolution and sorption of biochar (derived from different pyrolysis mechanisms with opposite spatial distribution of redox-active moieties) in HA solutions by elucidating the molecular changes of HA constituents, and provides the evidence of preferential sorption and HA-enhanced dissolution, and reveals the redistribution of redox-active molecules, which can add insights into the redox effects in biochar applicated environments.

Abbreviations
EEC   Electron exchange capacities
EDC   Electron-donating capacities

Li *et al. Carbon Research*   (2024) 3:26

Page 12 of 13

EAC	Electron-accepting capacities
HA	Humic acid
DOC	Dissolved organic carbon
EEM	Excitation–emission matrix
SPE	Solid-phase extraction
UPLC Orbitrap MS	Ultra-performance liquid chromatography coupled with Orbitrap mass spectrometry
XPS	X-ray photoelectron spectroscopy
ABTs	(2,2'-Azino-bis(3-ethylbenzothiazoline-6-sulfonic acid) diammonium salt
MW	Molecular weight
AImod	Modified aromaticity index
DBE	Double bond equivalence
NOSC	Nominal oxidation state of carbon

Supplementary Information

The online version contains supplementary material available at https://doi.org/10.1007/s44246-024-00110-7.

Additional file 1: Text S1. Mediated electrochemical measurement. **Text S2.** Molecular information analysis. **Text S3.** Formula categories. **Text S4.** Molecular index equations. **Text S5.** Calculation of sorption percentage. **Fig. S1.** Temporal evolution of DOC during sorption and dissolution processes. a) and b) Total DOC; c) and d) DOC after deducting that of dissolved biochar in control groups. **Fig. S2.** EEM contours of the fluorescent component. a) and the loading plot b) Ex: excitation Em: emission. **Fig. S3.** van Krevelen diagrams of HA stock solution and filtrates in equilibrium a) ESI+ b) ESI-. **Fig. S4.** Count of formulas in HA stock solution and filtrates in equilibrium a) categorized by elements b) categorized by van Krevelen diagrams. **Fig. S5.** Relative intensity of molecules in HA stock solution and filtrates in equilibrium a) categorized by elements b) categorized by van Krevelen diagrams. **Fig. S6.** Raw data of current response during EAC test of suspension. a) pi500 and b) st700. **Fig. S7.** Raw data of current response during EDC test of suspension. a) pi500 and b) st700. **Fig. S8.** Raw data of current response during EAC test of filtrates. a) pi500 and b) st700. **Fig. S9.** Raw data of current response during EEC test of HA stock solution. **Fig. S10.** C 1s, O 1s and N 1s XPS spectra of biochar. **Table S1.** The atomic proportion (obtained by XPS) and BET specific area of pristine biochar. **Table S2.** Peak area-weighted averages of molecular indexes for HA stock solution and filtrates at equilibrium. **Table S3.** The classification of sorbed and dissolved molecules.

Authors' contributions
All authors contributed to the study conception and design. Material preparation, data collection and analysis were performed by Shasha Li. The first draft of the manuscript was written by Shasha Li and all authors commented on previous versions of the manuscript. All authors read and approved the final manuscript.

Availability of data and materials
The datasets generated during and/or analysed during the current study are available from the corresponding author on reasonable request.

Declarations

Competing interests
The authors have no relevant financial or non-financial interests to disclose.

Author details
[1]State Key Laboratory of Pollution Control and Resource Reuse, Tongji University, Shanghai 200092, People's Republic of China. [2]Shanghai Institute of Pollution Control and Ecological Security, Shanghai 200092, People's Republic of China. [3]Institute of Waste Treatment and Reclamation, Tongji University, Shanghai 200092, People's Republic of China.

References

Aeschbacher M, Graf C, Schwarzenbach RP, Sander M (2012) Antioxidant properties of humic substances. Environ Sci Technol 46(9):4916–4925. https://doi.org/10.1021/es300039h

Aeschbacher M, Sander M, Schwarzenbach RP (2010) Novel electrochemical approach to assess the redox properties of humic substances. Environ Sci Technol 44(1):87–93. https://doi.org/10.1021/es902627p

Bahureksa W, Tfaily MM, Boiteau RM, Young RB, Logan MN, McKenna AM, Borch T (2021) Soil organic matter characterization by Fourier transform ion cyclotron resonance mass spectrometry (FTICR MS): A critical review of sample preparation, analysis, and data interpretation. Environ Sci Technol 55(14):9637–9656. https://doi.org/10.1021/acs.est.1c01135

Chen B, Zhou D, Zhu L (2008) Transitional adsorption and partition of nonpolar and polar aromatic contaminants by biochars of pine needles with different pyrolytic temperatures. Environ Sci Technol 42(14):5137–5143. https://doi.org/10.1021/es8002684

Chen W, Yang H, Chen Y, Li K, Xia M, Chen H (2018) Influence of biochar addition on nitrogen transformation during copyrolysis of algae and lignocellulosic biomass. Environ Sci Technol 52(16):9514–9521. https://doi.org/10.1021/acs.est.8b02485

Chiou CT, Cheng J, Hung W-N, Chen B, Lin T-F (2015) Resolution of adsorption and partition components of organic compounds on black carbons. Environ Sci Technol 49(15):9116–9123. https://doi.org/10.1021/acs.est.5b01292

Chun Y, Sheng G, Chiou CT, Xing B (2004) Compositions and sorptive properties of crop residue-derived chars. Environ Sci Technol 38(17):4649–4655. https://doi.org/10.1021/es035034w

Cruz Viggi C, Simonetti S, Palma E, Pagliaccia P, Braguglia C, Fazi S, Baronti S, Navarra MA, Pettiti I, Koch C, Harnisch F, Aulenta F (2017) Enhancing methane production from food waste fermentate using biochar: The added value of electrochemical testing in pre-selecting the most effective type of biochar. Biotechnol Biofuels 10(1):303. https://doi.org/10.1186/s13068-017-0994-7

Dittmar T, de Rezende CE, Manecki M, Niggemann J, Coelho Ovalle AR, Stubbins A, Bernardes MC (2012) Continuous flux of dissolved black carbon from a vanished tropical forest biome. Nat Geosci 5(9):618–622. https://doi.org/10.1038/ngeo1541

Dittmar T, Koch B, Hertkorn N, Kattner G (2008) A simple and efficient method for the solid-phase extraction of dissolved organic matter (SPE-DOM) from seawater. Limnol Oceanogr Methods 6(6):230–235. https://doi.org/10.4319/lom.2008.6.230

Guilayn F, Benbrahim M, Rouez M, Crest M, Patureau D, Jimenez J (2020) Humic-like substances extracted from different digestates: First trials of lettuce biostimulation in hydroponic culture. Waste Manage 104:239–245. https://doi.org/10.1016/j.wasman.2020.01.025

Guo P, Zhang CF, Wang Y, Yu XW, Zhang ZC, Zhang DD (2018) Effect of long-term fertilization on humic redox mediators in multiple microbial redox reactions. Environ Pollut 234:107–114. https://doi.org/10.1016/j.envpol.2017.10.106

Hagemann N, Joseph S, Schmidt HP, Kammann CI, Harter J, Borch T, Young RB, Varga K, Taherymoosavi S, Elliott KW, McKenna A, Albu M, Mayrhofer C, Obst M, Conte P, Dieguez-Alonso A, Orsetti S, Subdiaga E, Behrens S, Kappler A (2017) Organic coating on biochar explains its nutrient retention and stimulation of soil fertility. Nat Commun 8(1):1089. https://doi.org/10.1038/s41467-017-01123-0

Han L, Nie X, Wei J, Gu M, Wu W, Chen M (2021) Effects of feedstock biopolymer compositions on the physiochemical characteristics of dissolved black carbon from lignocellulose-based biochar. Sci Total Environ 751:141491. https://doi.org/10.1016/j.scitotenv.2020.141491

He M, Xu Z, Hou D, Gao B, Cao X, Ok YS, Rinklebe J, Bolan NS, Tsang DCW (2022) Waste-derived biochar for water pollution control and sustainable

development. Nat Rev Earth Environ 3(7):444–460. https://doi.org/10.1038/s43017-022-00306-8

Kasozi GN, Zimmerman AR, Nkedi-Kizza P, Gao B (2010) Catechol and humic acid sorption onto a range of laboratory-produced black carbons (biochars). Environ Sci Technol 44(16):6189–6195. https://doi.org/10.1021/es1014423

Kaudal BB, Weatherley AJ (2018) Agronomic effectiveness of urban biochar aged through co-composting with food waste. Waste Manage 77:87–97. https://doi.org/10.1016/j.wasman.2018.04.042

Klüpfel L, Keiluweit M, Kleber M, Sander M (2014) Redox properties of plant biomass-derived black carbon (biochar). Environ Sci Technol 48(10):5601–5611. https://doi.org/10.1021/es500906d

Kujawinski EB, Behn MD (2006) Automated analysis of electrospray ionization Fourier transform ion cyclotron resonance mass spectra of natural organic matter. Anal Chem 78(13):4363–4373. https://doi.org/10.1021/ac0600306

Lee S, Roh Y, Koh DC (2019) Oxidation and reduction of redox-sensitive elements in the presence of humic substances in subsurface environments: a review. Chemosphere 220:86–97. https://doi.org/10.1016/j.chemosphere.2018.11.143

Lehmann J, Cowie A, Masiello CA, Kammann C, Woolf D, Amonette JE, Cayuela ML, Camps-Arbestain M, Whitman T (2021) Biochar in climate change mitigation. Nat Geosci 14(12):883–892. https://doi.org/10.1038/s41561-021-00852-8

Li SS, Lü F, Zhang H, Shao LM, He PJ (2023) Electron exchange capacities of colloidal biochar: Affected by spatial structure distribution instead of particle size. Chem Eng J 455:140567. https://doi.org/10.1016/j.cej.2022.140567

Li SS, Shao LM, Zhang H, He PJ, Lü F (2020) Quantifying the contributions of surface area and redox-active moieties to electron exchange capacities of biochar. J Hazard Mater 394:122541. https://doi.org/10.1016/j.jhazmat.2020.122541

Lipczynska-Kochany E (2018) Humic substances, their microbial interactions and effects on biological transformations of organic pollutants in water and soil: A review. Chemosphere 202:420–437. https://doi.org/10.1016/j.chemosphere.2018.03.104

Murphy KR, Stedmon CA, Graeber D, Bro R (2013) Fluorescence spectroscopy and multi-way techniques PARAFAC. Analyt Methods 5(23):6557–6566. https://doi.org/10.1039/C3AY41160E

Qi H, Wang J, Zhang L, Chen L, Zhao Y, Wei Z (2022) Activation effect of catechol on biotic and abiotic pathways of humus formation during chicken manure composting. Waste Manage 149:146–155. https://doi.org/10.1016/j.wasman.2022.06.014

Qiu JJ, Lü F, Zhang H, Liu WY, Chen JL, Deng YT, Shao LM, He PJ (2020) UPLC Orbitrap MS/MS-based fingerprints of dissolved organic matter in waste leachate driven by waste age. J Hazard Mater 383:121205. https://doi.org/10.1016/j.jhazmat.2019.121205

Qu X, Fu H, Mao J, Ran Y, Zhang D, Zhu D (2016) Chemical and structural properties of dissolved black carbon released from biochars. Carbon 96:759–767. https://doi.org/10.1016/j.carbon.2015.09.106

Shaker MA, Albishri HM (2014) Dynamics and thermodynamics of toxic metals adsorption onto soil-extracted humic acid. Chemosphere 111:587–595. https://doi.org/10.1016/j.chemosphere.2014.04.088

Shao LM, Deng YT, Qiu JJ, Zhang H, Liu WY, Bazienė K, Lü F, He PJ (2021) DOM chemodiversity pierced better performance of each tandem unit along a full-scale "MBR+NF" process for mature landfill leachate treatment. Water Res 195:117000. https://doi.org/10.1016/j.watres.2021.117000

Shao LM, Li SS, Cai J, He PJ, Lü F (2019) Ability of biochar to facilitate anaerobic digestion is restricted to stressed surroundings. J Clean Prod 238:117959. https://doi.org/10.1016/j.jclepro.2019.117959

Shi Y, Hu H, Ren H (2020) Dissolved organic matter (DOM) removal from biotreated coking wastewater by chitosan-modified biochar: adsorption fractions and mechanisms. Biores Technol 297:122281. https://doi.org/10.1016/j.biortech.2019.122281

Smith CR, Hatcher PG, Kumar S, Lee JW (2016) Investigation into the sources of biochar water-soluble organic compounds and their potential toxicity on aquatic microorganisms. ACS Sustain Chem Engine 4(5):2550–2558. https://doi.org/10.1021/acssuschemeng.5b01687

Smith CR, Sleighter RL, Hatcher PG, Lee JW (2013) Molecular characterization of inhibiting biochar water-extractable substances using electrospray ionization Fourier transform ion cyclotron resonance mass spectrometry.

Environ Sci Technol 47(23):13294–13302. https://doi.org/10.1021/es4034777

Song F, Li T, Shi Q, Guo F, Bai Y, Wu F, Xing B (2021) Novel insights into the molecular-level mechanism linking the chemical diversity and copper binding heterogeneity of biochar-derived dissolved black carbon and dissolved organic matter. Environ Sci Technol 55(17):11624–11636. https://doi.org/10.1021/acs.est.1c00083

Song F, Li T, Wu F, Leung KMY, Hur J, Zhou L, Bai Y, Zhao X, He W, Ruan M (2023) Temperature-dependent molecular evolution of biochar-derived dissolved black carbon and its interaction mechanism with polyvinyl chloride microplastics. Environ Sci Technol 57(18):7285–7297. https://doi.org/10.1021/acs.est.3c01463

Stedmon CA, Bro R (2008) Characterizing dissolved organic matter fluorescence with parallel factor analysis: a tutorial. Limnol Oceanogr Methods 6(11):572–579. https://doi.org/10.4319/lom.2008.6.572

Subdiaga E, Harir M, Orsetti S, Hertkorn N, Schmitt-Kopplin P, Haderlein SB (2020) Preferential sorption of tannins at aluminum oxide affects the electron exchange capacities of dissolved and sorbed humic acid fractions. Environ Sci Technol 54(3):1837–1847. https://doi.org/10.1021/acs.est.9b04733

Subdiaga E, Orsetti S, Haderlein SB (2019) Effects of sorption on redox properties of natural organic matter. Environ Sci Technol 53(24):14319–14328. https://doi.org/10.1021/acs.est.9b04684

Sun T, Levin BDA, Guzman JJL, Enders A, Muller DA, Angenent LT, Lehmann J (2017) Rapid electron transfer by the carbon matrix in natural pyrogenic carbon. Nat Commun 8:14873. https://doi.org/10.1038/ncomms14873

Taherymoosavi S, Verheyen V, Munroe P, Joseph S, Reynolds A (2017) Characterization of organic compounds in biochars derived from municipal solid waste. Waste Manage 67:131–142. https://doi.org/10.1016/j.wasman.2017.05.052

Varga M, Izak T, Vretenar V, Kozak H, Holovsky J, Artemenko A, Hulman M, Skalova V, Lee DS, Kromka A (2017) Diamond/carbon nanotube composites: Raman, FTIR and XPS spectroscopic studies. Carbon 111:54–61. https://doi.org/10.1016/j.carbon.2016.09.064

Wang JG, Liu H, Sun H, Hua W, Wang H, Liu X, Wei B (2018) One-pot synthesis of nitrogen-doped ordered mesoporous carbon spheres for high-rate and long-cycle life supercapacitors. Carbon 127:85–92. https://doi.org/10.1016/j.carbon.2017.10.084

Wang W, Wang T, Liu Q, Wang H, Xue H, Zhang Z, Wang Y (2022) Biochar-mediated DNRA pathway of anammox bacteria under varying COD/N ratios. Water Res 212:118100. https://doi.org/10.1016/j.watres.2022.118100

Yang H, Ye S, Zeng Z, Zeng G, Tan X, Xiao R, Wang J, Song B, Du L, Qin M, Yang Y, Xu F (2020) Utilization of biochar for resource recovery from water: a review. Chem Eng J 397:125502. https://doi.org/10.1016/j.cej.2020.125502

Yu LP, Yuan Y, Tang J, Wang YQ, Zhou SG (2015) Biochar as an electron shuttle for reductive dechlorination of pentachlorophenol by Geobacter sulfurreducens. Sci Rep 5:16221. https://doi.org/10.1038/srep16221

Yuan Z, He C, Shi Q, Xu C, Li Z, Wang C, Zhao H, Ni J (2017) Molecular insights into the transformation of dissolved organic matter in landfill leachate concentrate during biodegradation and coagulation processes using ESI FT-ICR MS. Environ Sci Technol 51(14):8110–8118. https://doi.org/10.1021/acs.est.7b02194

Zhang B, Shan C, Wang S, Fang Z, Pan B (2021) Unveiling the transformation of dissolved organic matter during ozonation of municipal secondary effluent based on FT-ICR-MS and spectral analysis. Water Res 188:116484. https://doi.org/10.1016/j.watres.2020.116484

Publisher's Note